Available online at www.sciencedirect.com

SCIENCE DIRECT

Biochimica et Biophysica Acta 1664 (2004) 88–99

BIOCHIMICA ET BIOPHYSICA ACTA BBA

www.bba-direct.com

Evidence for heterodimers of 2,4,5-trichlorophenol on planar lipid layers. A FTIR-ATR investigation

Monira Siam[a], Gerald Reiter[a], René Hunziker[b], Beate Escher[c], Alfred Karpfen[d], Alexandra Simperler[e], Dieter Baurecht[a], Urs Peter Fringeli[a,*]

[a] *Institute of Physical Chemistry, University of Vienna, Althanstrasse 14, Vienna A-1090, Austria*
[b] *Dow Chemical, Zürich, Switzerland*
[c] *Swiss Federal Institute for Environmental Science and Technology, Dübendorf, Switzerland*
[d] *Institute for Theoretical Chemistry and Structural Biology, University of Vienna, Austria*
[e] *Institute for Organic Chemistry, University of Vienna, Austria*

Received 5 January 2004; received in revised form 8 April 2004; accepted 22 April 2004
Available online 18 May 2004

Abstract

Trichlorophenols are weak acids of high hydrophobicity and are able to transport protons across the mitochondrial membrane. Thus the proton motive force is dissipated and the ATP production decreased. In situ Fourier Transform Infrared-Attenuated Total Reflection (FTIR-ATR) experiments with 2,4,5-trichlorophenol (TCP) adsorbed to model membranes resulted in good evidence for the formation of the TCP-heterodimer. Two surfaces were examined: a dipalmitoyl phosphatidic acid (DPPA) monolayer and a planar DPPA/1-palmitoyl-2-oleoyl-*sn*-glycero-3-phosphocholine (POPC) bilayer. TCP was adsorbed from 1 to 3 mM solutions at pH 6.0 to the lipid layers leading to surface layers at the water/lipid interface. Difference spectra showed an effect on DPPA acyl chains even when it was covered with POPC. Time-resolved measurements revealed two distinct adsorption processes, which were assigned to TCP and its deprotonated anion (phenoxide), respectively. For DPPA/POPC bilayers, the adsorption of TCP was faster than that of its phenoxide, whereas adsorption of both species to DPPA monolayers proceeded with similar velocity. In both cases, phenoxide formation at the membrane was found to be delayed with respect to phenol adsorption. Phenoxide and phenol were retained after replacing the TCP solution with buffer. For the retained species, we estimated a phenol/phenoxide molar ratio of 1 at pH 6.0 ($pK_a = 6.94$ for TCP), demonstrating strong evidence for heterodimer formation.

Keywords: Model membrane; Uncoupling agent; 2,4,5-Trichlorophenol; Heterodimer; FTIR-ATR spectroscopy

1. Introduction

1.1. Chlorophenol–membrane interaction: narcosis and uncoupling

Chlorophenols are active components of a great number of pesticides. The quantities applied coupled with their long degradation times makes them a major class of environmental contaminants. In principle, their toxicity is caused either by a narcosis-based mechanism or by their respiratory uncoupling potential. Depending on the observed kinetics, class 1 and class 2 uncouplers can be differentiated. Class 1 uncouplers follow first-order kinetics, whereas for class 2 uncouplers second-order kinetics are found. Finkelstein [1] has proposed that class 2 uncouplers form heterodimers, consisting each of the neutral and the conjugated ionic species of the same substance. Indeed, for 2,4,5-trichlorophenol (TCP) second-order kinetics were determined based on experiments with energy-transducing membranes isolated from photosynthetic bacteria [2].

There exist a number of investigations comparing the toxicity of different substituted benzenes and phenols on various biological systems to elucidate quantitative structure–activity relationships (QSAR), e.g. [3–7]. The aim

* Corresponding author. Tel.: +43-1-4277-52530; fax: +43-1-4277-9525.
E-mail address: urs.peter.fringeli@univie.ac.at (U.P. Fringeli).

0005-2736/$ - see front matter © 2004 Elsevier B.V. All rights reserved.
doi:10.1016/j.bbamem.2004.04.006

of these studies was to find simple, reliable and general molecular descriptors, based on physical parameters like the octanol–water partition coefficient or the Hammett constant, which allows one to give an estimation of the toxicity of any compound without testing it in a living system. The more that is known concerning the mechanistic details of the interaction that affect the organism, the better is the chance to find the correct molecular descriptor.

Both narcosis and respiratory uncoupling are governed by the interaction between the compound and the cell membrane. Whereas narcotic agents alter the physical properties of cell membranes through incorporation, uncoupling agents permeate membranes and destroy the proton gradient essential for ATP production. As weak acids of high hydrophobicity, uncouplers transport protons across membranes via dissociation at the proton-poor side and proton uptake at the proton-rich side of the membrane [8,9]. From this point of view, the interaction of uncouplers with model membranes, like phospholipid vesicles, black lipid membranes and planar lipid layers, can be used to gain insight into the molecular mechanism of the narcotic effect [10,11] as well as of the uncoupling interaction.

In this paper, we report on an infrared spectroscopic study of the interaction of TCP with model membrane assemblies, using the technique of attenuated total reflection (ATR). This experimental method has turned out to be well-adapted for structural investigations of thin layers, such as supported biomembranes, on a molecular level [12–14]. Membrane preparation has been performed by means of the Langmuir–Blodgett (LB) or the LB/vesicle technique [15].

1.2. Kinetic schemes of uncoupling

In general, kinetic schemes of the uncoupling process consist of the following steps: (i) partitioning of the uncoupling agent into the membrane; (ii) translocation of the protonated species through the membrane; (iii) delivery of the proton at the interface of the side with the high pH; (iv) back diffusion across the membrane, and (v) uptake of protons at the interface from the side with the low pH to close the protonophoric shuttle.

It has been documented (e.g. in kinetic studies for substituted phenols [2,16]) that protonophoric uncouplers may exhibit first-order or second-order kinetics and, therefore, they are divided into class 1 and class 2 uncouplers. An explanation was given by Finkelstein [1] who proposed that the second-order kinetics are due to the formation of a heterodimer (AHA^-), e.g. consisting of a phenolic and a phenoxide entity for the chlorophenols. Through kinetic studies, Escher et al. [2] postulated that the heterodimer predominates the uncoupling process for TCP (Fig. 1). Therefore, we have chosen this compound for our Fourier Transform Infrared (FTIR)-ATR studies to assess the formation and existence of the phenol/phenoxide dimer by spectroscopic means.

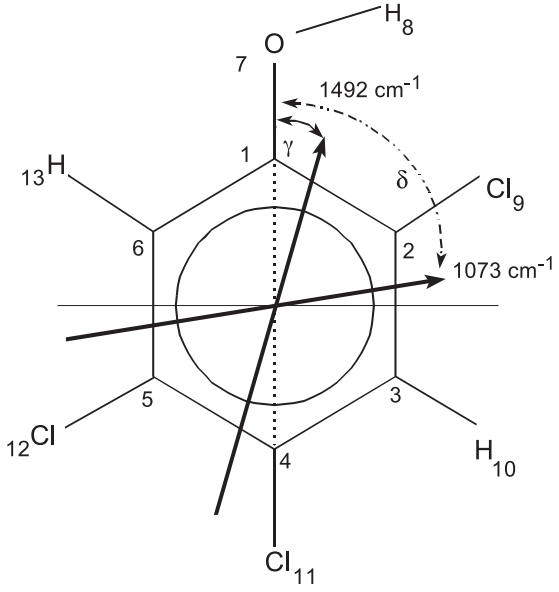

Fig. 1. Formula of TCP. The numbers of the atoms in the scheme refer to the interpretation of the potential energy distribution given in Table 3. The directions of transition dipole moments for 1492 cm^{-1} (calculated), 1488 cm^{-1} (experimental) and for 1073 cm^{-1} (calculated), 1080 cm^{-1} (experimental), as obtained from a potential energy distribution with BECKE3LYP/6–311++G(d, p), are indicated by arrows. Angles between transition dipole moments and the molecular axis O-C_1-C_4-Cl (dotted line) are denoted as γ(16°, 1492 cm^{-1}) and δ(81°, 1073 cm^{-1}).

2. Materials and methods

2.1. Materials

KOH, KCl, CCl_4 and *n*-hexane were obtained from Merck with p.a. grade. K_2HPO_4, KH_2PO_4, dipalmitoyl phosphatidic acid (DPPA) and 1-palmitoyl-2-oleoyl-*sn*-glycero-3-phosphocholine (POPC) were purchased from Fluka, whereas TCP came from Riedel-de Haën with 99% purity. HPLC analysis confirmed that the given specification was correct. The remaining 1% were mainly 2,4,6-trichlorophenol, tetrachlorophenols and dichlorophenols. Chemicals were used without further purification. Water used was purified with an Elga filtering system to give a specific resistance of 18.2 MΩ cm. The buffer employed was a 25 mM potassium phosphate buffer with a total concentration of 100 mM K^+ at pH 6.0.

2.2. Preparation of model membranes on internal reflection elements

At the beginning of an experiment, each side of the Ge plate used as multiple internal reflection element (MIRE) was polished by means of a 0.25 μm diamond paste for 10 min. Subsequently, the plate was cleaned with ultrapure

water and ethanol until there were no visible impurities left. In order to remove small traces of organic compounds, the Ge plate was cleaned for 3 min in a high-voltage glow discharge unit (Harrick Sci. Corp.). The Ge plate was considered to be clean if the CH_2-stretching bands ($\nu(CH_2)$) at ~ 2920 and ~ 2850 cm^{-1} disappeared completely in the FTIR-ATR spectrum (single-beam mode).

Monolayers were prepared by means of the LB technique described first by Blodgett [17] and later by Gaines [18]. About 25 μl of a 1 mg/ml DPPA solution in $CHCl_3$ was spread on a film balance (NIMA Technology, Coventry, UK) filled with an aqueous subphase containing 0.1 mM $CaCl_2$. After evaporation of the solvent, the film was compressed to a surface pressure of 30 mN/m and checked for stability for 5 min. The final area was about 100 cm^2, the MIRE area about 20 cm^2. Then the DPPA was transferred at (23 ± 2) °C and at a surface pressure of (30 ± 0.2) mN/m, withdrawing the Ge MIRE plate with a dipper speed of 2 mm/min (0.8 cm^2/min). The corresponding transfer ratio was (100 ± 3)%. Polarized FTIR-ATR spectra of the monolayer against air were recorded and quantitatively analyzed for surface concentration and orientation (reference: clean Ge in dry air). The checked DPPA-coated Ge MIRE was mounted in a single-beam-sample-reference (SBSR) [12–14,19,20] flow-through cell and filled with buffer for the subsequent experiments.

For the preparation of bilayers with POPC as outer leaflet, the LB/vesicle method [15] was used. A vesicle solution was prepared by sonification of the lipid in potassium phosphate buffer at pH 6.0. Two hundred microliters of a 10 mg/ml lipid/$CHCl_3$ solution was dried in a small glass tube and about 3 ml buffer were added to give a final lipid concentration of about 0.7 mg/ml. The solution was sonicated under N_2 purge for 30 min at temperatures above the chain melting temperature of POPC (25 °C < T < 32 °C). Solutions were almost completely transparent and used within 20 min. They were slowly pumped (0.2 ml/min) over a DPPA monolayer immobilized on the Ge plate. Then a bilayer was formed by spontaneous adsorption of lipid from small unilamellar vesicles at an adsorption temperature of 18 °C. Typically, the bilayer was completed after about 45 min. After 1 h, the vesicles solution was exchanged by buffer, and the temperature was raised to 25 °C for the following TCP experiments. Every step of the bilayer formation was monitored in situ by FTIR-ATR spectra. For typical spectra of DPPA and POPC, the reader is referred to Refs. [15,21].

2.3. Long-term measurements

For long-term measurements, a SBSR-ATR-setup with a chopper [19] was mounted in a BRUKER IFS 25 FTIR spectrometer. To prevent both the adsorption of TCP to hydrophobic surfaces and the contamination from softeners, a SBSR cell made of steel (flow-through cuvette) [20] and glass capillaries were used. The SBSR cell consisted of two compartments for each side of the Ge MIRE. The compartments were each of an area of 310.4 mm^2 and sealed from one another with Viton O-rings. TCP solutions of about 3 mM in buffer were prepared by sonication for 10 min and injected with a glass syringe. Spectra from adsorbed TCP in the presence and absence of TCP in the bulk phase were measured. For filling and washing with buffer solutions, a peristaltic pump (flow rate: 0.2 ml/min) was used.

2.4. Time-resolved measurements

TCP solutions of concentrations between 1 and 3 mM in buffer were prepared by sonication and pumped by means of a peristaltic pump (flow rate: 0.5 ml/min) over either a DPPA monolayer or a DPPA/POPC bilayer (for characterization see Section 3.3). A test of tube materials revealed that TCP did not adsorb to Viton. Time-resolved experiments with Viton tubes were carried out twice, the first time with a conducting connection between the Ge plate and the steel lid, the second time with an insulation of the Ge plate. Potentials were measured at the end of experiments and found to be 0 V for the first case and -0.42 and -0.34 V for the insulated plate with DPPA monolayer and DPPA/POPC bilayer, respectively.

Time-resolved measurements were performed during 0.5 h with a BRUKER IFS66 making use of a software controlled polarizer which allowed recording of parallel and perpendicular polarized spectra (15 each in turn) at intervals of 1 min. The adsorption was monitored until equilibrium was reached and documented with a SBSR-ATR spectrum. This was achieved with a SBSR-ATR lift attachment, as described in Refs. [13,14]. Afterwards, the TCP solution was exchanged for buffer, the adsorbate was washed for about 15 min and a SBSR-ATR spectrum was then scanned.

During the whole experiment, the pH and the concentration of TCP were monitored. The solutions were pumped with a peristaltic pump through the SBSR-ATR cell. Then they passed an optical concentration control unit (CCU) and a micro-flow-through pH electrode (Hamilton/Orion). The CCU consisted of a flow-through cell (standard IR-CaF_2 transmission cell with a 200 μm spacer) mounted in a micro-UV–VIS mirror attachment [20] located in the sample compartment of the FTIR instrument. Light transfer was performed by waveguides to a diode array UV–VIS spectrometer (Zeiss SPECORD S10). In order to protect the waveguides, a D_2 filter was used to block light in the range between 190 and 215 nm.

For the analysis of the time-resolved spectra with respect to TCP adsorption, peak heights at 1352 and 1080 cm^{-1} in parallel and perpendicular polarized spectra were determined. In order to get a numerical relation between surface concen-

tration and time of TCP interaction, data from series were fitted with a function $f(t)$ of one of the following types:

$$f(t) = g(1 - \exp(-kt))$$
$$f(t) = d + g(1 - \exp(-kt))$$
$$f(t) = d + g(1 - \exp(-kt)) + lt$$

(g... scaling factor, d... offset, k... rate constant, l... slope). No attempt was made to develop and analyze an adequate kinetic model. Numerical analysis was made with SigmaPlot 3.0. The type of $f(t)$ was chosen by trial and error to give the best fit (smallest Rsqr value). Usually, data points up to 1000 min were acquired by many short-term measurements of parallel and perpendicular polarization in turn. The time delay between succeeding parallel and perpendicularly polarized spectra was corrected by using interpolated data for the perpendicular polarization gained from the fitted curves. The results were used to calculate the surface concentration Γ and the dichroic ratio R for the bands at 1352 cm^{-1} (indicating strongly bound phenoxide) and at 1080 cm^{-1} (indicating loosely bound phenol) as a function of time. Quantification of the influence of TCP on the lipid layer was performed by integrating the symmetric CH_2-stretching vibrations, $\nu_s(CH_2)$, at 2850 cm^{-1}. To determine the time dependence, data were fitted with functions of the type $f(t) = d + g\exp(-kt)$.

2.5. Determination of molar absorption coefficients

2.5.1. IR transmission and IR-ATR measurements

Molar absorption coefficients for the typical bands of the two species of TCP were first determined from transmission measurements of solutions at pH 3 and pH 11. Therefore, TCP was dissolved either in diluted HCl or diluted KOH to give concentrations between 0.5 and 3 mM. Transmission measurements were performed with a CaF_2 cell using a 10 μm mylar spacer. The coefficients were refined by repeating the experiment in potassium phosphate buffer at pH 6.0. Curve fitting was used to separate the intense 1450 cm^{-1} band. Fitting parameters were checked to give the correct phenol/phenoxide ratios, calculated from the dissociation constant pK 6.94 [22]. ATR measurements of TCP solutions at pH 6.0 by means of a clean Ge MIRE were used to determine molar absorption coefficients, too, and to check for nonspecific adsorption to the MIRE surface. Peak and integrated molar absorption coefficients are summarized in Table 1.

2.5.2. UV–VIS

A 2.5 ml quartz cuvette with 1 cm pathlength was filled with 1800–1980 μl buffer and measured as reference. As standards for calibration 20–200 μl of a TCP stock solution were injected with a pipette to give concentrations in the range of 10–100 μM. The molar absorption coefficients were evaluated for the peak heights at the wavelengths given in Section 3.1. TCP solutions of concentrations in the millimole range were measured with a IR standard cuvette with CaF_2 windows and either a 0.1 or a 0.2 mm spacer for keeping the intense signals at 203 nm below one absorbance unit. UV–VIS measurements were performed at room temperature by means of a diode array spectrometer (Zeiss Specord S10) between 200 and 700 nm with 200 accumulations using an integration time of 50 ms and a resolution of 2.4 nm.

Table 1
Molar peak absorption coefficients and integrated molar absorption coefficients of bands characteristic for phenol and phenoxide

Position $\tilde{\nu}$/cm^{-1}	Assignment[a]	$\varepsilon(\tilde{\nu})/10^5$ cm^2 mol^{-1}	$\int\varepsilon(\tilde{\nu})d\tilde{\nu}/10^5$ cm mol^{-1}	Integration method
1080($HA_{ads.}$) 1080($HA_{diss.}$)	HA	1.85 ± 0.08	7.2 ± 0.6	1085–1074 cm^{-1}[b]
1352 ($A^-_{ads.}$)	A^-	1.5 ± 0.2	14 ± 2	1361–1340 cm^{-1}[c]
1456 ($A^-_{diss.}$) 1446 ($A^-_{ads.}$)	A^-		288 ± 6	curve fitting[d] at 1456 cm^{-1}

$\varepsilon(\tilde{\nu})$ and $\int\varepsilon(\tilde{\nu})d\tilde{\nu}$ were determined by IR transmission experiments with the dissolved species $HA_{diss.}$ (at pH 3) or $A^-_{diss.}$ (at pH 11.3) except for 1352 cm^{-1} which is a characteristic band of adsorbed phenoxide $A^-_{ads.}$. In this case, $\varepsilon(\tilde{\nu})$ and $\int\varepsilon(\tilde{\nu})d\nu$ were determined by correlation with the corresponding band at 1446 cm^{-1}.

[a] Assignment according to normal coordinate analysis, see Section 3.2.1.

[b] Peak area above a linear baseline set between 1092 and 1067 cm^{-1}.

[c] Peak area above a linear baseline set between 1365 and 1337 cm^{-1}.

[d] Peak shape: Lorentzian, HW: 19.9 cm^{-1}.

3. Results

3.1. UV–VIS measurements

UV–VIS measurements were used to determine TCP concentrations in solution and to check for association at pH 6 and 11.3 as well as for oxidation in diluted KOH at pH 11.0–11.9. At pH 6.0, the UV spectra (not shown) revealed a small peak at 293 nm and an intense peak at 203 nm. In case of using the waveguides and the D_2 filter, the peak shoulder at 229 nm was evaluated instead of the peak at 203 nm. Deprotonation at pH 11.1 shifted these peaks to 312 and 209 nm, respectively, and a new peak emerged at 245 nm. A perfect Lambert–Beer behavior was found for TCP concentrations between 0.01 and 3.0 mM (in buffer at pH 6.0) and 0.03 and 3.0 mM (in diluted KOH at pH 11.3) when absorbance peak heights at the wavelengths given above were plotted against concentration. Therefore, association of TCP did not seem to occur in solutions up to 3 mM. Molar absorption coefficients are listed in Table 2.

In order to check phenol stability against oxidation, TCP dissolved in diluted KOH was exposed for 2.75 h to dry air bubbling through the solution at ambient temperature. Since no changes could be detected, we assumed that TCP solutions were stable within the duration of our experiments.

Table 2
Molar peak absorption coefficients ε from UV–VIS measurements[a]

pH	6.0	6.0	6.0	11.3	11.3	11.3
Wavelength (λ/nm)	203	229	293	209	245	312
ε (10^6 cm^2 mol^{-1})	37 ± 1	6.8 ± 0.5	2.5 ± 0.1	29 ± 2	9.0 ± 0.7	4.3 ± 0.2

[a] TCP dissolved in 25 mM K-phosphate buffer pH 6.0 or diluted KOH pH 11.3, respectively.

3.2. IR transmission measurements

3.2.1. Phenol and phenoxide spectra

Transmission spectra of TCP solutions of acidic and alkaline pH values were used to identify TCP as acid (HA) and as phenoxide (A^-). The results are shown in Fig. 2. At pH 11.3 (Fig. 2a), three intense absorption bands appear at 1456, 1367 and 1292 cm^{-1}, which are typical for the deprotonated state. These bands are absent at pH 3.0, i.e. in the protonated state of TCP (Fig. 2c), whereas broad bands exist around 1475 and 1400 cm^{-1} and the appearance of a sharp band at 1080 cm^{-1} is recognised. Based on these results, the ATR spectrum of TCP adsorbed to a DPPA/POPC bilayer at pH 6 (Fig. 2b) is to be interpreted as a superposition of the acid and phenoxide spectra. The bands at 1080, 1400 and 1488 cm^{-1} show the presence of HA, whereas the prominent peak at 1446 cm^{-1} is the major component of an overlapped band indicating, together with the band at 1045 cm^{-1}, the existence of phenoxide (A^-) in the membrane. This peak is paralleled by a smaller, but better resolved band at 1352 cm^{-1}, whereas the band corresponding to that of A^- in solution at 1292 cm^{-1} is too small to be significantly identified. However, a downward frequency shift of about 10 cm^{-1} of typical absorption bands of A^- is observed between dissolved and adsorbed

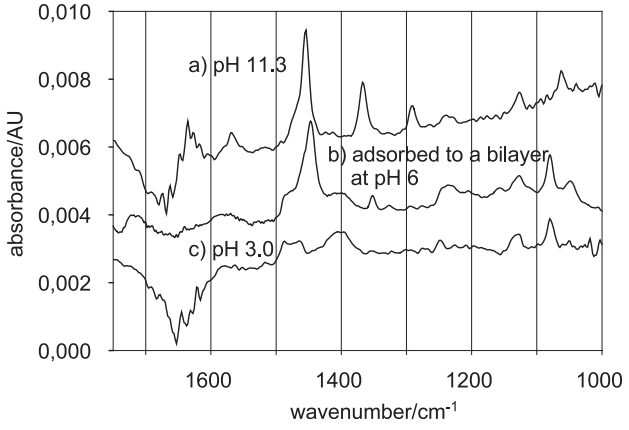

Fig. 2. Comparison of IR TR spectra of 3 mM TCP solutions at pH 11.3 and pH 3.0 with a parallel polarized ATR-IR spectrum of TCP adsorbed to a DPPA/POPC bilayer at pH 6. (a) 3 mM TCP in diluted KOH pH 11.3; (b) TCP adsorbing from a 2.9 mM solution in 25 mM potassium phosphate buffer pH 6 (c_{total} (K^+) = 100 mM) to a DPPA/POPC bilayer; (c) 3 mM TCP in diluted HCl pH 3.0. Peak shifts of about 10 wavenumbers between (a) and (b) may indicate changes in hydrogen bonding. TR measurement conditions: CaF_2 cuvette with d = 10 μm, ambient temperature; ATR measurements: Ge-MIRE, active reflections N_{act}=(18.4 ± 1), angle of incidence θ=(45 ± 1.5)°, T = 25 °C. The ATR spectrum was scaled down by a factor of 0.2.

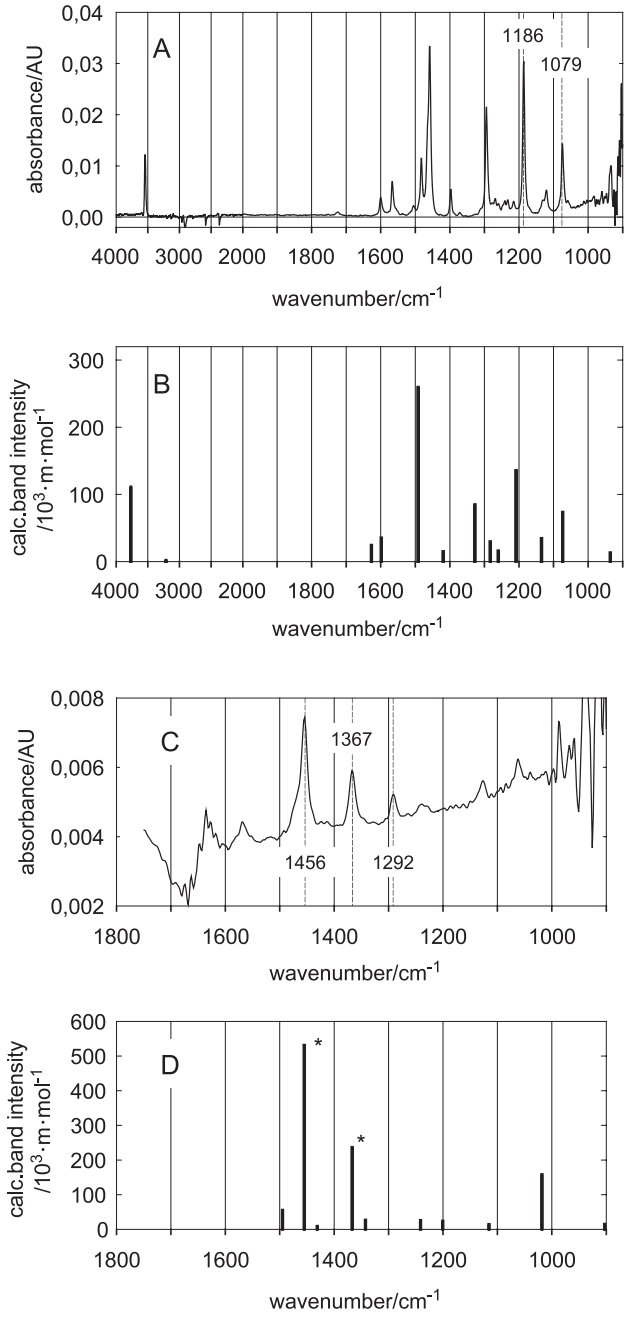

Fig. 3. Experimental and calculated IR spectra of TCP. (A) Absorbance TR-IR spectra of 10 mM TCP in CCl_4 (measurement conditions: CaF_2 cuvette, pathlength 50 μm, ambient temperature). (B) IR band intensities ($\int\varepsilon(\tilde{\nu})d\tilde{\nu}$) as calculated with BECKE3LYP/6–311++G(d, p). Experimental and calculated IR spectra of 2,4,5-trichlorophenoxide. (C) Absorbance TR-IR spectrum of 3 mM TCP in 2 mM KOH (measurement conditions: CaF_2 cuvette, pathlength 10 μm, ambient temperature). (D) IR band intensities ($\int\varepsilon(\tilde{\nu})d\tilde{\nu}$) as calculated with BECKE3LYP/6–311++G(d, p). Frequencies marked by an asterisk (*) were shifted down (1605 cm^{-1}/−150 cm^{-1}, 1549 cm^{-1}/−180 cm^{-1}) to fit the experimental data, taking a possible dimerization of K^+-phenoxide complexes into account [25].

phenoxide (compare Fig. 2a with Fig. 2b). We interpret these downward shifts as strengthening of hydrogen bonds to A^- in the membrane and as a possible hint for heterodimer formation because the mere water hydrogen bonding to A^- in solution could be replaced by intermolecular HA hydrogen bonding to A^- in the membrane. It should be noted, though, that the measurements of A^- in solution were performed at pH 11.3 in order to get spectra of pure A^-, whereas the measurements of A^- in the membrane were obtained at pH 6, i.e. at a pH value where the phenol HA would dominate over A^- in solution. Pronounced phenoxide formation at pH 6.0 was typical for lipid layers and could be detected neither on clean Ge nor on clean ZnSe surfaces. Furthermore, signals of TCP in bulk solution were so small compared to adsorbed TCP that their contribution could be neglected.

Compared with the TCP spectra in Fig. 2, the FTIR spectrum of TCP dissolved in CCl_4 (Fig. 3A) reveals a significant sharpening of absorption bands. The peak at 1186 cm^{-1} should be mentioned, since it is very prominent in CCl_4, but strongly reduced or even erased in aqueous environment. This sensitivity to the environment gives evidence that the OH group is also involved in this vibration as confirmed by vibrational analysis (Table 3).

For assignment of bands and for the estimation of the direction of their transition dipole moments, we performed quantum chemical calculations with the GAUSSIAN 98 [23] suites of programs to get the normal modes of TCP. Therefore, geometry optimization was executed at the B3LYP level of density function theory (DFT) with a 6–311++G(d,p) basis set. The output was read by the program gar2ped (gaussian results to potential energy distribution) [24], which was used to calculate the normal modes and the potential energy distributions. The measured frequencies for TCP in CCl_4 (Fig. 3A) matched well with the calculated ones (Fig. 3B), thus giving confidence in calculated transition dipole moments used for orientation analysis. The potential energy distributions are presented in Table 3.

However, assignments for the phenoxide (A^-) are not as straightforward because DFT is known to poorly describe even simple phenoxide [25]. This might result from solvent effects or from interaction with counterions: the complexation and dimerization may lead to downshifts in the order of 100 cm^{-1} for vibrations containing significant amounts of ν(CO) [26]. This was also the case for the 2,4,5-trichlorophenoxide measured in diluted KOH. Therefore, we decided to shift down the frequencies 1605 to 1456 cm^{-1} and 1549 to 1369 cm^{-1}, both with a high percentage of ν(CO). The results are shown in Fig. 3D and are in good agreement with the experimental intensity pattern in Fig. 3C.

Table 3
Experimental and calculated[a] wavenumbers for TCP

A_{max} (exp.)/ cm^{-1}	Also found at/cm^{-1}	A_{max} (calc.)/ cm^{-1}	$\int \varepsilon^{th}(\tilde{\nu})d\tilde{\nu}^b /10^5$ cm mol^{-1}	Potential energy distribution[c]	Angle α(°)
1079	1080[d]/1074[e]	1073	74	δ(ring) 49%, − $\nu(C_2Cl)$ 16%, $\nu(C_6C_1)$ 8%, $\nu(C_2C_1)$ 7%	81
1130	1128[e]	1135	35	$\nu(C_4C_5)$ 19%, δ(CH) 18%+14% (−), − $\nu(C_4Cl)$ 13%, $\nu(C_5C_6)$ 10%, − $\nu(C_5Cl)$ 9%	–
1186		1208	136	$\delta(C_1OH)$ 37%, $\nu(C_1C_{6,2})$ 17%+9% (−), − δ(CH) 13%+6%	25
1248		1260	16	δ(CH) 25%+23%?, − $\nu(C_4C_3)$ 23%, − $\nu(C_1C_2)$ 8%, $\delta(C_1OH)$ 7%	–
		1283	30	$\nu(C_1O)$ 31%, − $\nu(C_2C_3)$ 29%, $\delta(C_3H)$ 11%, − $\nu(C_4C_5)$ 8%	–
		1327	85	$\nu(C_5C_6;C_2C_3)$ 23%+10%(−), − $\nu(C_4C_{5,3})$ 18%+10%(−), $\delta(C_1OH)$ 14%, $\nu(C_1C_2)$ 10%, − $\nu(C_1O)$ 5%	–
1400		1419	15	$\nu(C_5C_6)$ 19%, $\delta(C_1OH)$ 16%, − $\nu(C_4C_3)$ 14%, $\nu(C_1O)$ 7%, − $\nu(C_2C_3)$ 7%	–
1488		1492	260	$\delta(C_3H)$ 22%, − $\delta(C_6H)$ 15%, − $\nu(C_2C_3)$ 12%, $\nu(C_1O)$ 11%, $\nu(C_4C_{5,3})$ 10%+8%(−), $\nu(C_1C_{6,2})$ 8%+6%(−)	16
1565[e]		1599			
1600[e]		1627			
		3212/3214		$\nu(CH_{13,10})$: 89%+10%(−)	
		3767		ν(OH) 100%	

Potential energy distribution and the angle α between the transition dipole moment and the molecular axis OC_1C_4Cl are given.
[a] Quantum chemical calculation (BECKE3LYP/6–311++G(d, p)).
[b] Calculated band intensity.
[c] Numbers of atoms refer to Fig. 1, ν for stretching, δ for bending, − for out of phase vibrations.
[d] 25 mM potassium phosphate buffer.
[e] *n*-hexane and CCl_4.

3.2.2. Molar peak absorption coefficients and integrated molar absorption coefficients

In case of interaction with the DPPA monolayer and the DPPA/POPC bilayer, the band at 1080 cm^{-1} is taken as a measure for adsorbed phenolic TCP. According to normal coordinate analysis (Table 3), this band results from a combined vibration containing 49% of C–C bending ("ring breathing") and 16% C–Cl stretching as major components. For the determination of the integrated molar absorption coefficient $\int \varepsilon(\tilde{\nu})d\tilde{\nu}$, IR transmittance spectra of solutions containing TCP concentrations between 0.5 and 3 mM at pH 3.0 were used. The corresponding band area was obtained by integration from 1085 to 1074 cm^{-1} using a linear baseline as indicated in Table 1. Peak heights were found to be less influenced by the baseline and the signal-to-noise ratio. Therefore, the molar peak absorption coefficient $\varepsilon(\tilde{\nu})$ at 1080 cm^{-1} was also determined from peak heights measured with respect to a straight baseline between 1092 and 1067 cm^{-1}. This absorption coefficient was used for calculation of surface concentrations of phenolic HA adsorbed to DPPA monolayers and DPPA/POPC bilayers.

The 1352 cm^{-1} band was chosen for quantitative analysis of the phenoxide A^- (see also Section 3.2.1). $\int \varepsilon(\tilde{\nu})d\tilde{\nu}$ and $\varepsilon(\tilde{\nu})$ of this band were determined with respect to a straight baseline between 1365 and 1337 cm^{-1}. The integration was performed within 1361 and 1340 cm^{-1}. Quantification of TCP adsorbates from time-resolved measurements were determined from peak heights at 1352 cm^{-1}. A summary of applied parameters is given by Table 1.

3.3. Characterization of the prepared model membranes

The first leaflet of the membrane consisted always of a DPPA monolayer transferred from the air/water interface to the surface of a Ge MIRE. The procedure is described, e.g. in Refs. [15,21]. Quantitative analysis of the $\nu_s(CH_2)$ band according to Ref. [14] resulted in a surface concentration of $\Gamma=(3.85 \pm 0.30) \times 10^{-10}$ mol/cm^2, which is based on an integrated molar absorption coefficient of $\nu_s(CH_2)$ of $\int \varepsilon(\tilde{\nu})d\tilde{\nu}=(5.70 \pm 0.20) \times 10^5$ cm/mol using a linear baseline between (2830 ± 1) and (2869 ± 1) cm^{-1}. The corresponding molecular cross-section of a DPPA molecule was then calculated to $A_{DPPA}=(43.2 \pm 3.0)$ $Å^2$/molecule. The molecular order parameter S_{mol} is found to be close to 1.00 which means nearly perfect (x,y)-orientation for the transition dipole moments of $\nu_s(CH_2)$ and z-orientation of the molecular axis, i.e. of the hydrocarbon chains. These results are in very good agreement with those reported by Demel et al. [27], who determined 43.8 $Å^2$ per molecule at the air/water interface at pH 7.0.

The second lipid layer of the membrane consisted of POPC and was transferred by means of the LB/vesicle method [15,21]. Applying the same analytical methods as for DPPA resulted in a molecular cross-section of (94 ± 15) $Å^2$, pointing to a rather loosely packed layer, since corresponding data from literature are found to be within 68 and 70 $Å^2$/molecule [28].

3.4. Long-term measurements of lipid–TCP interaction

3.4.1. Interaction of TCP with DPPA monolayers

Fig. 4 displays SBSR absorbance spectra of 2.9 mM TCP adsorbed to a DPPA monolayer after 1 h (a) and 12 h (b) of exposure at pH 6. The prominent peak at 1446 cm^{-1} is accompanied by shoulders at 1487 and 1462 cm^{-1}. Spectra (a) and (b) display a broad shoulder at 1400 cm^{-1} as well as smaller well resolved bands at 1352, 1327, 1238, 1127, 1080 and 1048 cm^{-1}. The broad band near 1650 cm^{-1} reflects a small incompensation of the water δ(OH) band. Obviously, adsorption of TCP to the hydrophobic surface of the DPPA monolayer is completed within the first hour. The adsorbed layer turned out to be extremely stable, since only small amounts of predominantly HA could be washed out by buffer solution, as revealed by traces c and d of Fig. 4.

3.4.2. Interaction of TCP with DPPA/POPC bilayers

The FTIR-ATR-SBSR absorbance spectra of a DPPA/POPC bilayer after exposure to TCP for 16 h with and without TCP in the bulk phase are shown in Fig. 5a and b, respectively. Prominent bands of TCP are localized at

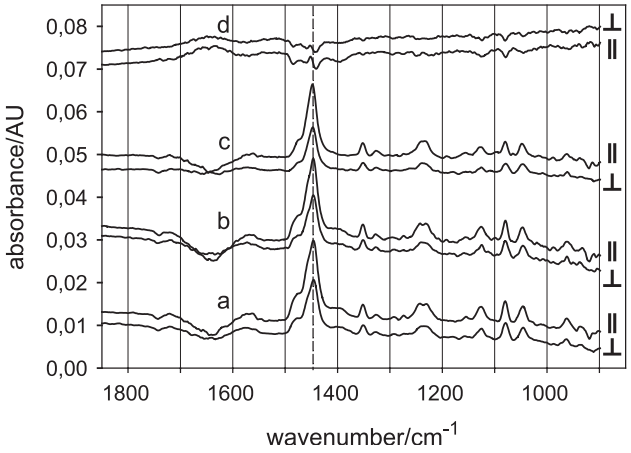

Fig. 4. Polarized IR-ATR absorbance spectra between 1850 and 900 cm^{-1} of TCP adsorbed to a DPPA monolayer. Parallel (∥) and perpendicular (⊥) polarized spectra after 1 (a) and 12 h (b) exposure of the monolayer to a 2.9 mM 2,4,5-TCP solution at pH 6.0. (c) TCP solution replaced by 25 mM potassium phosphate buffer pH 6.0 (c_{total} (K^+) = 100 mM). A prominent peak at 1446 cm^{-1} dominates the spectrum and is typical for the phenoxide (A^-). (d) The difference spectrum c–b shows only a small decrease of phenoxide, but about 1/3 loss of phenol (1400, 1080 cm^{-1}) by washing with buffer. Surface concentrations after washing turned out to be $\Gamma_{HA}=(4.8 \pm 0.9) \times 10^{-10}$ mol/cm^2 and $\Gamma_{A^-}=(5.9 \pm 0.9) \times 10^{-10}$ mol/cm^2 resulting in a HA/A^- ratio of (0.81 ± 0.20). Measurement conditions: trapezoidal Ge MIRE, angle of incidence $\theta=(45 \pm 1.5)°$, active internal reflections $N_{act}=(16.15 \pm 1)$; refractive indices: $n_1=4.0$ (Ge), $n_2=(1.50 \pm 0.05)$ (membrane), $n_3=(1.31 \pm 0.05)$ (H_2O, 1446 cm^{-1}) used for calculation of Γ_{A^-}, and $n_3=(1.26 \pm 0.05)$ (H_2O, 1080 cm^{-1}) used for calculation of Γ_{HA}.

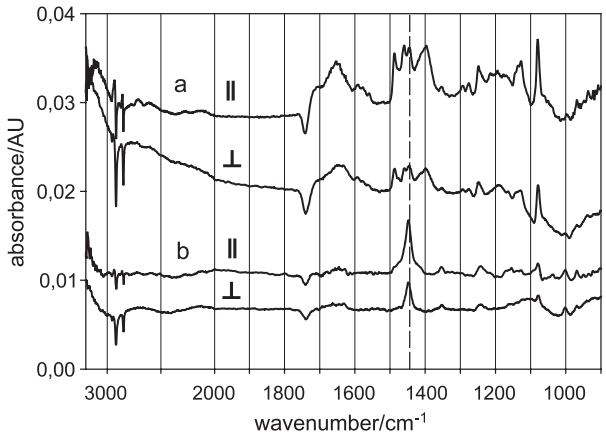

Fig. 5. Comparison of polarized IR-ATR absorbance spectra of a lipid bilayer in contact (a) and after the contact (b) with a 2.9 mM TCP solution (exposure time: 16 h). (a) Parallel (∥) and perpendicular (⊥) polarized spectra of the DPPA/POPC bilayer. Calculated surface concentrations for phenol (TCP (HA); 1080 cm^{-1}) and phenoxide (TCP^- (A^-); 1446 cm^{-1}): $\Gamma_{HA} = (1.14 \pm 0.22) \times 10^{-9}$ mol/cm^2 and $\Gamma_{A^-}=(1.60 \pm 0.10) \times 10^{-10}$ mol/cm^2. (b) TCP solution replaced with 25 mM potassium phosphate buffer pH 6 (c_{total} (K^+) = 100 mM). The peak at 1446 cm^{-1} indicates phenoxide and is marked with a dashed line. Calculated surface concentrations for phenol (TCP (HA); 1080 cm^{-1}) and phenoxide (TCP^- (A^-); 1446 cm^{-1}): $\Gamma_{HA}=(1.6 \pm 0.3) \times 10^{-10}$ mol/cm^2 and $\Gamma_{A^-}=(1.9 \pm 0.2) \times 10^{-10}$ mol/cm^2 resulting in a HA/A^- ratio of (0.84 ± 0.18). Thus AHA^- heterodimers may be retained in or on the bilayer. Measurement conditions: trapezoidal Ge MIRE, angle of incidence $\theta=(45 \pm 1.5)°$; active internal reflections $N_{act}=(18.4 \pm 1)$; refractive indices: $n_1 = 4.0$ (Ge), $n_2=(1.50 \pm 0.05)$ (membrane), $n_3=(1.31 \pm 0.05)$ (H_2O, 1446 cm^{-1}) used for calculation of Γ_{A^-} and $n_3=(1.26 \pm 0.05)$ (H_2O, 1080 cm^{-1}) used for calculation of Γ_{HA}.

1487, 1462, 1400, 1248, 1200, 1127 and 1080 cm^{-1}. A band at 1446 cm^{-1} appeared with increasing time. Replacing the TCP buffer solution by pure buffer led to spectra b of Fig. 5. Most primarily observed bands of TCP have vanished to a great extent, except the 1446 cm^{-1} band. A pure DPPA/POPC bilayer in contact with buffer served as reference (SBSR mode). The C–H stretching regions exhibited significant differences with respect to the shapes of parallel polarized (∥) and perpendicular (⊥) polarized spectra. Sigmoidal band shapes appeared with ∥-polarized light, while ⊥-polarized light led to negative CH_2-stretching bands. The corresponding minima of the $\nu_{as}(CH_2)$ and $\nu_s(CH_2)$ are found at 2919 and 2850 cm^{-1}, respectively, i.e. closer to the wavenumbers observed with DPPA ($\nu_{as}(CH_2)$: 2917 cm^{-1}; $\nu_s(CH_2)$: 2850 cm^{-1}) than with POPC ($\nu_{as}(CH_2)$: 2923 cm^{-1}; $\nu_s(CH_2)$: 2853 cm^{-1}). Furthermore, negative bands at 1741 cm^{-1} (ν(C=O), ester group) and at about 1100 cm^{-1} (superposition of $\nu_s(PO_2^-)$ and ν(P–O–C), phosphatidic acid/ester group) can be detected; band assignments of phospholipids are found, e.g. in Ref. [29]. Since this effect is considerably reduced upon washing the membrane with buffer, the observed negative bands cannot be interpreted as lipid loss but rather as hydrocarbon chain reorientation (see Section 4.1). As in the case of TCP adsorbed to a DPPA monolayer, adsorption to the DPPA/POPC bilayer results in two forms of bound TCP, a loosely bound one, which can be washed out easily, and a tightly bound one, which was not affected by washing.

3.5. Time-resolved measurements of lipid–TCP interaction

3.5.1. Interaction with DPPA monolayers

The adsorption of TCP to DPPA monolayers was monitored in situ with parallel and perpendicular polarized spectra for concentrations between 1 and 3 mM. Since this experiment was performed in a stainless steel SBSR flow-through cuvette, the Ge MIRE assumed a negative potential of −0.42 V. The corresponding experiment under short-circuit condition led to the same results within the limits of confidence of ±20%. The band at 1446 cm^{-1} (with its shoulders) increased together with the peaks at 1352, 1080 and 1048 cm^{-1}. The latter three have molar absorption coefficients of similar magnitude, whereas the molar absorption coefficient for 1446 cm^{-1} is found to be larger (see Table 1). At equilibrium (after 1 h, Fig. 4a) the two peaks at 1080 and 1048 cm^{-1} reached about the same size. At the beginning, however, the band at 1080 cm^{-1} was dominant. As depicted by Fig. 6, the determination of the surface concentrations Γ(HA) and $\Gamma(A^-)$ revealed that HA reached its saturation value somewhat faster than A^-. The surface

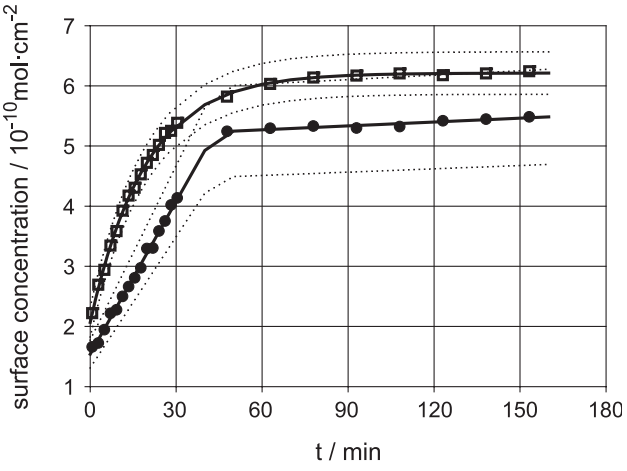

Fig. 6. Calculated surface concentrations of phenol (HA, open squares) and phenoxide (A^-, filled circles) on a DPPA monolayer vs. time. The peak heights at 1080 cm^{-1} (HA) and 1352 cm^{-1} (A^-) were used to calculate the surface concentration Γ. Curves represent interpolations of experimental values. Reference spectrum: DPPA monolayer against buffer. Molar absorption coefficients: ε(HA (1080 cm^{-1})) = $(1.85 \pm 0.08) \times 10^5$ cm^2mol^{-1}, $\varepsilon(A^-$ (1352 cm^{-1})$=(1.5 \pm 0.2) \times 10^5$ cm^2mol^{-1}. The dotted lines represent the standard deviations of the curves (includes standard deviation of fit parameters and of the molar absorption coefficient). At equilibrium $\Gamma_{HA}=(6.2 \pm 0.4) \times 10^{-10}$ mol/cm^2 and $\Gamma_{A^-}=(5.5 \pm 0.8) \times 10^{-10}$ mol/cm^2, resulting in a phenol to phenoxide ratio of $\Gamma_{HA}/\Gamma_{A^-} = 1.1 \pm 0.2$. Measurement conditions: Ge trapezoid MIRE (U = −0.42 V; Ge MIRE as negative pole), angle of incidence $\theta=(45 \pm 1.5)°$, active internal reflections $N_{act}=(13.5 \pm 1)$, T = 25 °C, concentration of TCP c_{sol}: 2.1 mM, refractive indices: $n_1 = 4.0$ (Ge), $n_2=(1.50 \pm 0.05)$ (membrane), $n_3=(1.31 \pm 0.05)$ (H_2O, 1352 cm^{-1}) and $n_3=(1.26 \pm 0.05)$ (H_2O, 1080 cm^{-1}).

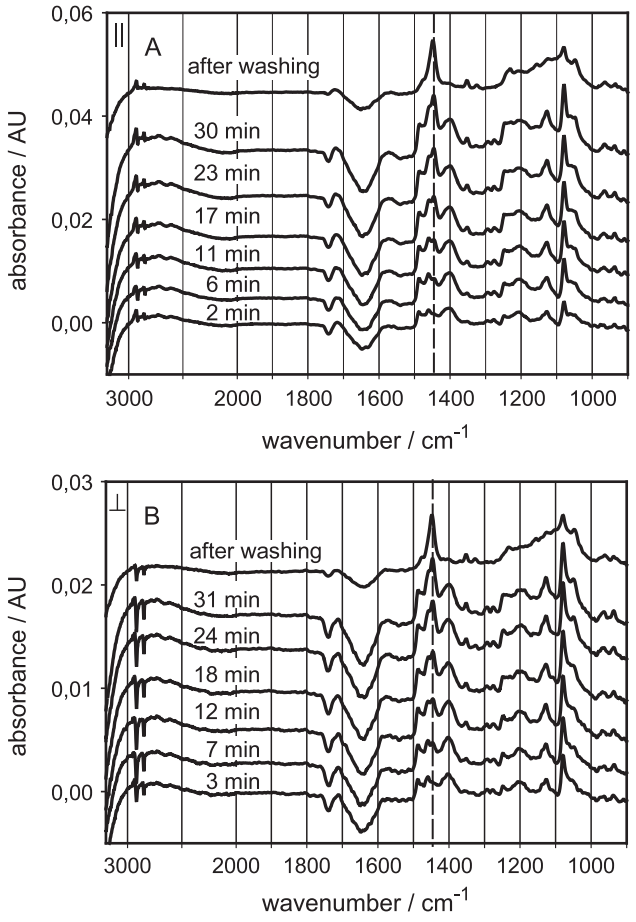

Fig. 7. Time-resolved IR-ATR absorbance spectra of the adsorption of TCP to a DPPA/POPC bilayer. A TCP solution (c_{TCP}=2.0 mM) in 25 mM potassium phosphate buffer pH 6.0 (c_{total} (K^+)=100 mM) was pumped into a flow-through cell at 0.5 ml/min and 25°C. For 0.5 h parallel (∥) and perpendicular (⊥) polarized ATR spectra were measured in turn every 64 s. After about 1 h, the TCP solution was exchanged for buffer and the adsorbate was washed for 15 min. (A) Parallel (∥) polarized absorbance spectra of the washed adsorbate (top) and time-resolved series of the adsorption process. (B) Perpendicular (⊥) polarized spectra arranged as in panel (A). A dashed line marks a peak emerging at 1446 cm^{-1} which is typical for the phenoxide (A^-). Reference: DPPA/POPC bilayer against 25 mM potassium phosphate buffer pH 6.0 (c_{total} (K^+)=100 mM). Measurement conditions: Ge trapezoid MIRE, angle of incidence θ=(45 ± 1.5)°, active internal reflections N_{act}=(13.5 ± 1).

concentrations were calculated using peak heights at 1080 and 1352 cm^{-1}, respectively. Corresponding molar absorption coefficients are indicated in Table 1. Time-resolved data as presented in Fig. 6 were interpolated (solid lines) by a function $f(t)=d+g(1-\exp(-kt))+lt$, where d, g, k and l are fitting parameters describing offset, maximal contribution of the exponential term, rate constant of adsorption and slope of a very slow continued adsorption of TCP, respectively. One may conclude a phenol to phenoxide ratio $\Gamma_{HA}/\Gamma_{A^-}=1.1\pm0.2$ as soon as equilibrium is approached where $\Gamma_{HA}=(6.2\pm0.4)\times10^{-10}$ mol/cm^2 and $\Gamma_{A^-}=(5.5\pm0.8)\times10^{-10}$ mol/cm^2. The rate constants for adsorption of TCP to the hydrophobic side of a DPPA monolayer were found to be $k(A^-)=(0.035\pm0.005)$ min^{-1} for the phenoxide and $k(HA)=(0.05\pm0.01)$ min^{-1} for the phenol.

3.5.2. Interaction of TCP with DPPA/POPC bilayers

In Fig. 7A and B ATR spectra measured during the exposure of 2 mM TCP to a DPPA/POPC bilayer are shown. The first spectrum of the time course was acquired after 2 min (Fig. 7A, lowest trace). It looks very similar to the spectrum of TCP at pH 3 (Fig. 2c), i.e. the phenol HA. However, already after about 5 min a sharp new band emerged at 1446 cm^{-1} and became the prominent component of the complex band between 1500 cm^{-1} and 1360 cm^{-1}. A corresponding small, but well resolved band appeared at 1352 cm^{-1}, and could be used for kinetic analysis of the formation of this new species which, according to Fig. 2a, must be assigned to the phenoxide A^- of TCP.

As in the case of TCP interaction with a DPPA monolayer, there is a significant effect on the structure of the hydrocarbon chains. A band shift to slightly higher wavenumbers is observed with symmetric and asymmetric CH_2-stretching in the ∥-polarized spectra (Fig. 7A); corresponding negative bands were observed in the ⊥-polarized spectra (Fig. 7B). Both polarizations feature negative bands of the C=O stretching vibration at 1740

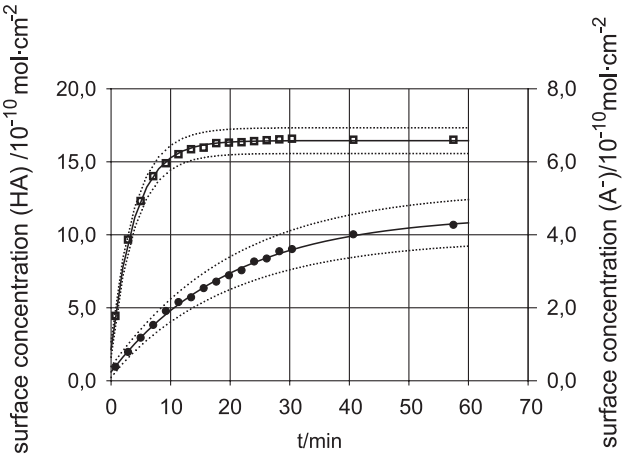

Fig. 8. Calculated surface concentrations Γ for phenol and phenoxide on a DPPA/POPC bilayer vs. time. Open squares denote values for Γ(HA) and refer to the left axis, whereas filled circles indicate values for $\Gamma(A^-)$, referring to the right axis. Peak heights A_{max} at 1080 cm^{-1} for Γ(HA) and a molar absorption coefficient of $\varepsilon=(1.85\pm0.08)\times10^5$ cm^2/mol, as well as peak heights A_{max} at 1352 cm^{-1} for $\Gamma(A^-)$ with $\varepsilon=(1.5\pm0.2)\times10^5$ cm^2/mol were used. Data from the peak heights were fitted with $f(t)=d+g(1-\exp(-kt))$ in order to calculate the equilibrium surface concentration $f(t=\infty)=d+g$, resulting in: $\Gamma_{HA}=(1.65\pm0.10)\times10^{-9}$ mol/cm^2 and $\Gamma_{A^-}=(0.43\pm0.07)\times10^{-9}$ mol/cm^2. Dotted lines represent the standard deviation of $\Gamma(t)$. Reference: DPPA/POPC bilayer against 25 mM potassium phosphate buffer pH 6.0 (c_{total} (K^+)=100 mM). Measurement conditions: Ge trapezoid MIRE, angle of incidence θ=(45 ± 1.5)°, active internal reflections N_{act}=(13.5 ± 1), T=25 °C, concentration of TCP c_{sol}: 2.0 mM, refractive indices: n_1=4.0 (Ge), n_2=(1.50 ± 0.05) (membrane), n_3=(1.31 ± 0.05) (H_2O, 1352 cm^{-1}) and n_3=(1.26 ± 0.05) (H_2O, 1080 cm^{-1}).

cm^{-1}. Surprisingly, these significant effects disappeared to a great extent as soon as TCP was replaced by washing with pure buffer solution. This procedure eliminated also a considerable amount of the phenol component HA, paralleled by the appearance of a very broad absorption between 1250 cm^{-1} and 1000 cm^{-1}. The time course was analyzed for HA by the band at 1080 cm^{-1} and for A^- by the band at 1352 cm^{-1}, using $f(t)=d+g(1-\exp(-kt))$ to fit the data. There was no significant difference in the k values obtained from parallel ($\parallel$) or perpendicular polarized ($\perp$) spectra. However, the two species HA and A^- showed quite different behavior. At 1080 cm^{-1} one obtained $k_{HA}=(0.255\pm0.03)$ min^{-1} and at 1352 cm^{-1} it followed $k_{A^-}=(0.053\pm0.01)$ min^{-1}. The time course of the adsorption of HA and A^- is depicted in Fig. 8. Note that in presence of a bulk TCP solution, there is a significantly higher surface concentration of the phenol (HA, left-hand scaling) than of the phenoxide (A^-, right-hand scaling): The saturation concentrations determined by the extrapolation of the corresponding fitting functions $f(t)$ resulted in $\Gamma_{HA}=(1.65\pm0.10)\times10^{-9}$ mol/cm^2 and $\Gamma_{A^-}=(0.43\pm0.07)\times10^{-9}$ mol/cm^2, respectively.

4. Discussion

4.1. Stacks and multilayer formation

To visualize the amount of TCP adsorbed to the layers, surface concentrations of TCP monolayers have been calculated from the molecular size of TCP. The size was estimated from interatomic distances O_7-Cl_{11} (9.31 Å) and Cl_9-Cl_{12} (9.87 Å), resulting from geometry optimization, considering a van der Waals' radius of Cl of 1.8 Å. We assumed the same size for phenol and phenoxide and an overall shape of an elliptic cylinder for the molecules. Then a maximum and a minimum area per molecule were estimated as $A_{max}=62.5$ $Å^2$ (benzene ring parallel to the plane of the membrane surface) and $A_{min}=10.2$ $Å^2$ (benzene ring perpendicular to the plane of the membrane surface). Therefore, the surface concentration of a monolayer of TCP (both entities together) could be between 2.7×10^{-10} and 1.6×10^{-9} mol/cm^2, depending on the orientation of the molecules.

In case of direct interaction of TCP with DPPA (Fig. 4) after washing with buffer, one obtained for $\Gamma_{HA}=(4.8\pm0.9)\times10^{-10}$ mol/cm^2 and for $\Gamma_{A^-}=(5.9\pm0.9)\times10^{-10}$ mol/cm^2 leading to a $\Gamma_{total}=\Gamma_{HA}+\Gamma_{A^-}=(1.07\pm0.13)\times10^{-9}$ mol/cm^2 and a HA/A^- ratio of (0.81 ± 0.20). However, TCP interaction with a DPPA/POPC bilayer (Fig. 5) resulted in $\Gamma_{HA}=(1.6\pm0.3)\times10^{-10}$ mol/cm^2 and for $\Gamma_{A^-}=(1.9\pm0.2)\times10^{-10}$ mol/cm^2 leading to a $\Gamma_{total}=(3.5\pm0.4)\times10^{-10}$ mol/cm^2 and a HA/A^- ratio of (0.84 ± 0.18). Since in the former case there is no tendency of TCP multilayer formation at elevated exposure times, we conclude that the spectrum shown in Fig. 4c is representative for a monolayer containing HA and A^- orienting the planes of benzene rings approximately normal to the plane of the membrane surface.

We suggest that this is similar with the DPPA/POPC bilayer. In this case, however, HA adsorbed spontaneously to the hydrophilic surface of POPC and penetrated with slower kinetics into the membrane (see Fig. 8). On such a path TCP will be hindered by POPC, which was partly ($\sim$15%) displaced by TCP (see Fig. 5b), leading to a delayed formation and to a reduced surface concentration of tightly bound TCP. As revealed by Fig. 5, there exist two different populations of TCP bound to the bilayer. Still in presence of bulk phase TCP one observes a significant excess of the phenol HA which, however, turned out to be only loosely bound in the major part, since about 85% HA detached from the membrane upon replacing bulk phase TCP by pure buffer. The remaining tightly bound TCP revealed a phenol/phenoxide ratio of $\Gamma_{HA}/\Gamma_{A^-}=0.84\pm0.18$ 0.18 (see above). This finding gives strong evidence for heterodimer formation in the membrane as reported in Refs. [1,2]. Finally, it should be noted that loosely bound TCP exerts a reversible structural effect on the lipid bilayer as revealed by the sigmoidal band shapes of $\nu_s(CH_2)$ and $\nu_{as}(CH_2)$ in Fig. 5a ($\parallel$) and the corresponding negative bands in Fig. 5a ($\perp$). The latter as well as the negative bands of $\nu(C=O)$ at 1740 cm^{-1} reflect only a minor amount of lipid loss, since this effect vanishes to a great extent after washing out. The significant structural effects on hydrocarbon chains and fatty acid ester groups of the lipid membrane are thus most probably exerted from outside the membrane. Since $\nu(CH_2)$ bands are shifted to higher wavenumbers, we postulate the formation of gauche defects in the hydrocarbon chains, leading to reorientation of the ester groups by interaction with loosely bound TCP. Electrostatic effects initiated at the membrane surface may play a role.

4.2. Orientation analysis

The approximate directions of transition dipole moments were calculated from the normal mode analysis with respect to the O-C_1-C_4-Cl axis. The results for two prominent vibrations of HA are shown in Fig. 1.

On the DPPA monolayer, TCP adsorbed and deprotonated rapidly and led to a $\sim$1:1 phenol/phenoxide layer. For the orientation analysis of the phenol (HA) the bands at 1080 and at 1488 cm^{-1} were used. Phenoxide (A^-) orientation measurements were based on the bands at 1352 and 1045 cm^{-1}. Dichroic ratios for the 1080 cm^{-1} band started with $R^{iso}=1.44\pm0.12$ (isotropic thin film) and increased to 1.6–1.7 within an exposure time of about 1 h and concentrations of 2–3 mM. For the 1352 cm^{-1} band ($R^{iso}=1.53\pm0.14$), dichroic ratios leveled off at 1.7–1.8. Based on the dichroic ratio of $R=1.7\pm0.14$ for 1080 cm^{-1} at equilibrium, we determined a mean angle (α) between the z-axis (normal to the membrane surface) and the corresponding transition

dipole moments of $\alpha=(49.4 \pm 1.3)^\circ$ [14]. Taking the angle between the O-C_1-C_4-Cl axis of the HA molecule and the transition dipole moment into account, which was found to be 81° for the calculated frequency of 1073 cm^{-1} (Fig. 1), the O-C_1-C_4-Cl axis encloses an angle of about 30° with the *z*-axis.

Considering the interaction of TCP with the DPPA/POPC membrane, one observed first a fast oriented adsorption to the membrane surface. This is concluded from time-resolved dichroic ratios of the 1080 cm^{-1} band, which resulted in $R=1.90 \pm 0.14$ ($R^{iso}=1.44 \pm 0.12$) from the beginning. Corresponding measurements with the 1352 cm^{-1} band resulted in $R=1.85 \pm 0.15$ ($R^{iso}=1.53 \pm 0.14$).

For HA, calculation based on the dichroic ratio of $R=1.90 \pm 0.14$ for 1080 cm^{-1} at equilibrium led to a resulting mean angle $\alpha=(46.3 \pm 1.2)^\circ$. After subtraction from the calculated angle of 81° between the O-C_1-C_4-Cl axis of the HA molecule and the transition dipole moment, a mean angle between the *z*-axis and the O-C_1-C_4-Cl axis of the TCP entity of about 35° is obtained, which is almost the same orientation as found for TCP on DPPA monolayers.

4.3. Conclusions

Experimental and theoretical data presented in this paper give strong evidence that TCP exposed at pH 6 penetrates a bilayer membrane and dissociates partly to form tightly bound 1:1 complexes, so-called heterodimers. This process was suggested earlier based on membrane conductance experiments [1] and kinetic measurements [2]. To our knowledge, this is the first time that strong spectroscopic evidence for the existence of a 1:1 phenol/phenoxide complex is given.

At pH 6 the phenol/phenoxide ratio in the bulk phase is calculated from $pK_a=6.94$ to be 10. Very surprisingly, spontaneous heterodimer formation occurs at the hydrophobic surface of a DPPA monolayer. Orientation measurements and determination of the surface concentration revealed an oriented, tightly packed monolayer featuring an angle of about 30° between the O-C_1-C_4-Cl axis (see Fig. 1) and the *z*-axis (normal to the membrane surface). Exposing a DPPA/POPC bilayer to the same bulk solution led to spontaneous oriented adsorption of the phenol to the surface of the bilayer. Most probably, due to the electrostatic interaction exerted to the membrane by adsorbed ionic species of TCP, reversible conformational changes occurred in the region of the hydrocarbon chains and of the fatty acid ester groups. It might be that TCP-induced gauche defects in the hydrocarbon chains enabled penetration of TCP into the interior of the membrane, forming again very tightly bound heterodimers in the hydrophobic environment, similar to the process observed with the DPPA monolayer, however, significantly slower and with a lower surface concentration corresponding to the loss of about 15% POPC of the outer monolayer of the membrane. Heterodimers remain trapped in the membrane, even when the bulk TCP solution is replaced by pure buffer. However, the structural disturbances in the hydrocarbon chains in the ester region vanish to the major part in this case. This observation might give some evidence for a proton shuttle enabling, e.g., decoupling of ATP synthesis. The orientation of the heterodimers in the bilayer is found to be the same as observed with the DPPA monolayer.

Acknowledgements

The authors thank Prof. René Schwarzenbach, EAWAG, CH-8600-Dübendorf (Switzerland) for continuous interest and support and Prof. Werner Mikenda, Institute of Organic Chemistry, University of Vienna for valuable discussions.

References

[1] A. Finkelstein, Weak-acid uncouplers of oxidative phosphorylation. Mechanism of action on thin lipid membranes, Biochim. Biophys. Acta 205 (1970) 1–6.
[2] B.I. Escher, M. Snozzi, R.P. Schwarzenbach, Uptake, speciation, and toxic effect of substituted phenols in energy transducing membranes, Environ. Sci. Technol. 30 (1996) 3071–3079.
[3] M.T.D. Cronin, Y.H. Zhao, R.L. Yu, pH-Dependence and QSAR analysis of the toxicity of phenols and anilines to *Daphnia magna*, Environ. Toxicol. 15 (2000) 140–148.
[4] T.W. Schultz, Structure–toxicity relationships for benzenes evaluated with *Tetrahymena pyriformis*, Chem. Res. Toxicol. 12 (1999) 1262–1267.
[5] M.A. Warne, A.A. Meharg, D. Osborn, J.C. Lindon, J.K. Nicholson, Quantitative structure toxicity relationships for halogenated substituted benzenes to *Vibrio fisheri* using atom-based J.K. semi-empirical molecular orbital descriptors, Chemosphere 38 (1999) 3357–3382.
[6] E. Argese, C. Bettiol, G. Giurin, P. Miana, Quantitative structure–activity relationships for the toxicity of chlorophenols to mammalian submitochondrial particles, Chemosphere 38 (1999) 2281–2292.
[7] A.P. Bearden, T.W. Schultz, Comparison of *Tetrahymena* and *Pimephales* toxicity based on mechanism of action, SAR QSAR Environ. Res. 9 (1998) 127–153.
[8] S.G.A. McLaughlin, J.P. Dilger, Transport of protons across membranes by weak acids, Physiol. Rev. 60 (1980) 825–863.
[9] H. Terada, Uncouplers of Oxidative-Phosphorylation, Environ. Health Perspect. 87 (1990) 213–218.
[10] M. Schöpflin, U.P. Fringeli, X. Perlia, A study on the interaction of local anesthetics with phospholipid model membranes by infrared ATR spectroscopy, J. Am. Chem. Soc. 109 (1987) 2375–2380.
[11] A. Shibata, K. Ikawa, H. Terada, Site of action of the local anesthetic tetracaine in a phosphatidylcholine bilayer with incorporated cardiolipin, Biophys. J. 69 (1995) 470–477.
[12] U.P. Fringeli, In situ infrared attenuated total reflection membrane spectroscopy, in: F.M. Mirabella (Ed.), Internal Reflection Spectroscopy, Marcel Dekker, New York, 1992, pp. 255–324.
[13] U.P. Fringeli, ATR and reflectance IR spectroscopy, applications, in: J.C. Lindon, G.E. Tranter, J.C. Holmes (Eds.), Encyclopedia of Spectroscopy and Spectrometry, Academic Press, San Diego, 1999, pp. 58–75.
[14] U.P. Fringeli, D. Baurecht, M. Siam, G. Reiter, M. Schwarzott, T. Bürgi, P. Brüesch, ATR spectroscopy of thin films, in: H.S. Nalwa (Ed.), Handbook of Thin Film Materials, vol. 2, Academic Press, San Diego, 2002, pp. 191–229, Chap. 4.

[15] P. Wenzl, M. Fringeli, J. Goette, U.P. Fringeli, Supported phospholipid bilayers prepared by the "LB/Vesicle Method": a Fourier transform infrared attenuated total reflection spectroscopic study on structure and stability, Langmuir 10 (1994) 4253–4264.
[16] B.I. Escher, R. Hunziker, R.P. Schwarzenbach, Kinetic model to describe the intrinsic uncoupling activity of substituted phenols in energy transducing membranes, Environ. Sci. Technol. 33 (1999) 560–570.
[17] K.B. Blodgett, Films built by depositing successive monomolecular layers on a solid surface, J. Am. Chem. Soc. 57 (1935) 1007–1022.
[18] G.L. Gaines Jr., Insoluble Monolayers at Liquid Gas Interfaces, Interscience, New York, 1966.
[19] U.P. Fringeli, J. Goette, G. Reiter, M. Siam, D. Baurecht, Structural Investigations of Oriented Membrane Assemblies by FTIR-ATR Spectroscopy, in: J.A. deHaseth (Ed.), Fourier Transform Spectroscopy: 11th International Conference, AIP Conf. Proceedings, vol. 430, American Institute of Physics, Woodbury, NY, 1998, pp. 729–747.
[20] Equipment was obtained from OPTISPEC, Rigistrasse 5, CH-8173 Neerach, Switzerland.
[21] G. Reiter, M. Siam, D. Falkenhagen, W. Gollneritsch, D. Baurecht, U.P. Fringeli, Interaction of a bacterial endotoxin with different surfaces investigated by in situ Fourier transform infrared attenuated total reflection spectroscopy, Langmuir 18 (15) (2002) 5761–5771.
[22] B.I. Escher, R.P. Schwarzenbach, Partitioning of substituted phenols in liposome–water, biomembrane–water, and octanol–water systems, Environ. Sci. Technol. 30 (1996) 260–270.
[23] M.J. Frisch, G.W. Trucks, H.B. Schlegel, C.E. Scuseria, M.A. Robb, J.R. Cheeseman, J.A. Zakrzewski , J.A. Montgomery Jr., R.E. Stratmann, J.C. Burant, S. Dapprich, J.M. Millam, A.D. Daniels, K.N. Kudin, M.C. Strain, O. Farkas, J. Tomasi, V. Barone, M. Cossi, R. Cammi, B. Mennucci, C. Pomelli, C. Adamo, S. Clifford, J. Ochterski, C.A. Petersson, P.Y. Ayala, Q. Cui, K. Morokuma, D.K. Malick, A.D. Rabuck, K. Raghavachari, J.B. Foresman, J. Cioslowski, J.V. Ortiz, B.B. Stefanov, G. Liu, A. Liashenko, P. Piskorz, I. Komaromi, R. Gomperts, R.L. Martin, D.J. Fox, T. Keith, M.A. Al-Laham, C.Y. Peng, A. Nanayakkara, C. Gonzalez, M. Challacombe, P.M. Gill, B. Johnson, W. Chen, M.W. Wong, J.L. Andres, C. Gonzalez, M. Headgle, E.S. Replogle, J.A. Pople, Gaussian 98, Revision A.6, Gaussian, Pittsburgh, PA, 1998.
[24] J.M.L. Martin, C. van Alsenoy, Gar2ped, University of Antwerpen, 1995.
[25] O. Nwobi, J. Higgins, X. Zhou, R. Liu, Density functional calculation of phenoxyl radical and phenolate anion: an examination of the performance of DFT methods, Chem. Phys. Lett. 272 (1997) 155–161.
[26] M. Nonella, H.U. Suter, Formation of phenolate anion–counterion complexes can explain the vibrational properties of the phenolate anion in solution, J. Phys. Chem., A 103 (1999) 7867–7871.
[27] R.A. Demel, C.C. Yin, B.Z. Lin, H. Hauser, Monolayer characteristics and thermal behaviour of phosphatidic acids, Chem. Phys. Lipids 60 (1992) 209–223.
[28] R.W. Evans, M.A. Willams, J. Tinoco, Surface areas of 1-palmitoyl phosphatidylcholines and their interactions with cholesterol, Biochem. J. 245 (1987) 455–462.
[29] U.P. Fringeli, Hs.H. Günthard, Infrared membrane spectroscopy, in: E. Grell (Ed.), Membrane Spectroscopy, Springer, Berlin, 1981, pp. 270–332.